Robust a Simulation for Shallow Flows with Friction on Rough Topography

Jian Deng[1], Ruo Li[2,*], Tao Sun[3] and Shuonan Wu[1]

[1] *School of Mathematical Sciences, Peking University, Beijing 100871, China.*
[2] *HEDPS & CAPT, LMAM & School of Mathematical Sciences, Peking University, Beijing 100871, China.*
[3] *Reservoir Characterization Division ExxonMobil Upstream Research Company, P. O. Box 2189 Houston, Texas 77252, USA.*

Abstract. In this paper, we propose a robust finite volume scheme to numerically solve the shallow water equations on complex rough topography. The major difficulty of this problem is introduced by the stiff friction force term and the wet/dry interface tracking. An analytical integration method is presented for the friction force term to remove the stiffness. In the vicinity of wet/dry interface, the numerical stability can be attained by introducing an empirical parameter, the water depth tolerance, as extensively adopted in literatures. We propose a problem independent formulation for this parameter, which provides a stable scheme and preserves the overall truncation error of $\mathscr{O}(\Delta x^3)$. The method is applied to solve problems with complex rough topography, coupled with h-adaptive mesh techniques to demonstrate its robustness and efficiency.

1. Introduction

Shallow water equations (SWEs) have been extensively applied to model hydrodynamic phenomena such as estuary and coastal tidal flows, bore wave propagation, surface irrigation, lake and reservoir hydrodynamics, and open channel flows. Although the numerical methods for shallow water equations have been studied thoroughly in the last decades, there are still some persistent difficulties in their application to practical models, which are often slightly different from the homogeneous shallow water equations. In the case of complex and rough topography, the differences under consideration here are very

---

*Corresponding author. *Email addresses:* `lyricidyll3@gmail.com` (J. Deng), `rli@math.pku.edu.cn` (R. Li), `tao.sun@exxonmobil.com` (T. Sun), `wsn1987@gmail.com` (S. N. Wu)

typical, including the friction force term of Manning form [1] due to the topography roughness, and the wet/dry interface due to wave propagating on a dry topography in practical applications.

The Manning friction force turns out to be a stiff source term in case of small water depth in the vicinity of wet/dry interface. As Bradford and Sanders [2] pointed out, the Manning formula requires division by water depth h, which results in an unrealistically large prediction of friction force in shallow regions near wet/dry interface, making the momentum equations stiff and the solution sensitive to water depth. Typical discretized methods have been applied to the friction source term, including the explicit Euler method [3,4], the implicit Euler method [5,6], and the semi-implicit method [7,8]. However, to keep the numerical stability and to control truncation error both impose more severe constraints on time step than the CFL condition. We apply the Strang splitting to separate the Manning friction force term from the shallow water equations, then give the analytical solution in the splitting step when handling the friction source term thus the constraint on time step due to the stiffness is released.

The other problems are the incorrect diffusion and the numerical sensitivity near wet/dry interface. The averaging process of data in a partially wetted cell at the wet/dry interface may give a very small water depth and wet the faces of this cell. As it is averaged on the entire cell instead of the wet part, artificial spreading of water into neighbour dry cells leads to the qualitatively incorrect wet/dry interface diffusing [2]. Furthermore, the small water depth makes the numerical scheme instable that additional error is produced. Many authors have studied the techniques for the wet/dry front. The positivity of the water height and the well-balance property under the presence of dry areas is achieved by two basic ingredients: a positivity reconstruction [9–11] and an additional time step constraint [12,13]. The basic idea of the latter method is to reduce the time step only for the edges that contribute to the outflow of these cells. We note that the new technique for treating wet/dry fronts in the context of Roe schemes presented in [11,14], which consists of an adequate nonlinear Riemann solver (exactly solved) at the intercells where a wet/dry transition has detected. In this work, we adopt the method in [9]. Precisely, the numerical errors of velocities u and v which are computed by $(hu)/h$ and $(hv)/h$ are amplified in case of $h \to 0$. As a remedy, an artificial parameter is prescribed in the numerical scheme by many authors [2,4,15–17], which is referred as *water depth tolerance* and denoted by h_{tol} later on. In case of water depth smaller than h_{tol}, the velocity components are set to be zero and the local fluxes are neglected to suppress possible instability. The numerical results therein illustrate that this technique works if magnitude of the parameter is appropriate. However, the value of the empirical parameter h_{tol} is problem dependent. If h_{tol} is chosen large enough to prevent wet/dry interface diffusion, the overall accuracy may be spoiled by the error on wet/dry interface. On the other hand, as reported in [2] and [16], h_{tol} has been varied by one order of magnitude higher and lower in a variety of frictionless problems with a negligible influence on the resulting solution. But for problems with bed friction of the Manning form, the model becomes even more sensitive to the value of h_{tol}. We remove the sensitivity by directly integrating the friction source term, and propose a problem independent formulation of h_{tol} preserving the overall truncation error of

$\mathcal{O}(\Delta x^3)$. Since the new formula of h_{tol} is dependent on the local spatial mesh size, it can be applied to h-type adaptive mesh method smoothly.

The rest of this paper is organized as follows. In Section 2, the shallow water equations with friction force on rough topography and the numerical scheme in the wet area are presented. In Section 3, we analyze the stiffness of friction source term and propose an analytical integration formula. In Section 4, we give the formulation of the empirical parameter h_{tol} which preserves the overall truncation error. A number of test cases are presented to validate the optimal numerical accuracy and stability of the scheme in Section 5 and finally conclusions are arrived at in the last Section.

2. Discretisation of the governing equations

The 2D shallow water equations with source terms are derived by depth-integrating the Reynolds-averaged Navier-Stokes equations, under the assumption of incompressible fluid and hydrostatic pressure distribution, with the vertical acceleration of water particles neglected [18]. It is formulated as

$$\frac{\partial \mathbf{U}}{\partial t} + \nabla \cdot \mathbf{F} = \mathbf{S}, \tag{2.1}$$

where t is time, $\mathbf{U} = (h, hu, hv)^T$, h is water depth and $(u, v)^T$ are vertically averaged flow velocities along the x and y directions, respectively. The flux vector $\mathbf{F} = (\mathbf{E}, \mathbf{G})$ is as

$$\mathbf{E} = \begin{pmatrix} hu \\ hu^2 + \frac{1}{2}gh^2 \\ huv \end{pmatrix}, \quad \mathbf{G} = \begin{pmatrix} hv \\ huv \\ hv^2 + \frac{1}{2}gh^2 \end{pmatrix}. \tag{2.2}$$

The source term $\mathbf{S} = \mathbf{S}_b + \mathbf{S}_f$ includes the bottom slope source term $\mathbf{S}_b$ and the friction source term $\mathbf{S}_f$

$$\mathbf{S}_b = \begin{pmatrix} 0 \\ -gh\dfrac{\partial z}{\partial x} \\ -gh\dfrac{\partial z}{\partial y} \end{pmatrix}, \quad \mathbf{S}_f = \begin{pmatrix} 0 \\ -C_D u\sqrt{u^2 + v^2} \\ -C_D v\sqrt{u^2 + v^2} \end{pmatrix}, \tag{2.3}$$

where $z(x, y)$ is riverbed elevation, C_D is bed roughness coefficient computed by the Manning formula $C_D = gn^2 h^{-1/3}$ [1]. The parameters involved include the gravity constant g and the Manning roughness coefficient n.

As the friction source term $\mathbf{S}_f$ may cause numerical instability in the vicinity of wet/dry interface (see Section 3), we apply the operator splitting method following [5, 19] to get

the following two systems

$$
\begin{cases}
\dfrac{\partial \mathbf{U}}{\partial t} + \nabla \cdot \mathbf{F} = \mathbf{S}_b, & \text{(2.4a)} \\[2ex]
\dfrac{\partial \mathbf{U}}{\partial t} = \mathbf{S}_f, & \text{(2.4b)}
\end{cases}
$$

which are denoted by operators $\mathscr{L}^I$ and $\mathscr{L}^F$ respectively

$$
\begin{cases}
\dfrac{\partial \mathbf{U}}{\partial t} = \mathscr{L}^I \mathbf{U}, & \text{(2.5a)} \\[2ex]
\dfrac{\partial \mathbf{U}}{\partial t} = \mathscr{L}^F \mathbf{U}. & \text{(2.5b)}
\end{cases}
$$

The Strang splitting scheme [20] for the SWEs (2.1) is formally written as

$$
\mathbf{U}(\mathbf{x}, t^n + \Delta t) = \exp\left(\frac{1}{2}\Delta t \mathscr{L}^F\right) \exp\left(\Delta t \mathscr{L}^I\right) \exp\left(\frac{1}{2}\Delta t \mathscr{L}^F\right) \mathbf{U}(\mathbf{x}, t^n), \qquad \text{(2.6)}
$$

with $\mathbf{x} = (x, y)$.

We will propose a direct integration method for Eq. (2.4b) in Section 3. The remaining part of this section is to introduce the cell-centered finite volume method [21] applied to Eq. (2.4a), which is a 2nd-order scheme of Godunov type. As a consequence, the resulting scheme (2.6) is of 2nd-order accuracy in both space and time.

Let $\mathscr{D}$ be the computational domain. At time t^n, the SWEs (2.1) only make sense in the wet area Ω, which is the part of $\mathscr{D}$ with positive water depth. The domain $\mathscr{D}$ is triangulated into a set of triangular cells denoting as τ_i to form an unstructured mesh $\mathscr{T} = \bigcup \tau_i$. In each cell τ_i, the conservative variables of SWEs are discretized as piecewise linear functions as

$$
\mathbf{U}^n\big|_{\tau_i}(\mathbf{x}) = \mathbf{U}_i^n + \nabla \mathbf{U}_i^n(\mathbf{x} - \mathbf{x}_i),
$$

where $\mathbf{U}_i^n = \left(h_i^n, (hu)_i^n, (hv)_i^n\right)^T$ is the cell mean value, $\nabla \mathbf{U}_i^n$ is the slope on τ_i and $\mathbf{x}_i$ is the barycenter of τ_i. With a prescribed parameter h_{tol}, the cell τ_i in the triangulation is called a wet cell if its mean water depth h_i^n is not less than h_{tol}. Otherwise, τ_i is called a dry cell. As the discretisation of the wet area Ω, Ω_h is defined as the union of the wet cells

$$
\Omega_h \triangleq \bigcup \left\{\tau_i;\ h_i^n \geq h_{tol}\right\}.
$$

In the finite volume discretisation below, we only compute the numerical flux on the boundary of the wet cells. On the common boundary of two dry cells, the numerical flux is neglected.

2.1. MUSCL-Hancock scheme

Applying Gauss's theorem to the integral form of Eq. (2.4a) over a cell τ_i, one obtains

$$\frac{\partial}{\partial t} \int_{\tau_i} \mathbf{U} dx + \int_{\partial \tau_i} \mathbf{F} \cdot \mathbf{n} ds = \int_{\tau_i} \mathbf{S}_b dx, \tag{2.7}$$

where $\mathbf{n}$ is the unit outer normal vector of τ_i. The MUSCL-Hancock method [21] achieves a 2nd order accuracy time discretisation consisting of a predictor step and a corrector step. In the predictor step,

$$\mathbf{U}_i^{n+1/2} = \mathbf{U}_i^n - \frac{\Delta t}{2|\tau_i|} \sum_{j=1}^{3} \int_{\partial \tau_{i,j}} \mathbf{F}(\mathbf{U}_{\text{in}}^n) \cdot \mathbf{n}_j ds + \frac{\Delta t}{2} \mathbf{S}_{b,i}^n, \tag{2.8}$$

where $\mathbf{U}_i$ are cell-averaged conservative variables on τ_i, $|\tau_i|$ is the area of τ_i, $\partial \tau_{i,j}$ is the j-th edge of τ_i with the unit outer normal as $\mathbf{n}_j$, and $\mathbf{S}_{b,i}$ is bed slope source term discretized by a centered scheme with the riverbed gradient given by reconstruction. The flux vector $\mathbf{F}(\mathbf{U}_{\text{in}}^n)$ is evaluated at each cell face $\partial \tau_{i,j}$ after piecewise linear reconstruction based on the mean values in its neighboring cells (see Subsection 2.2). In the corrector step,

$$\mathbf{U}_i^{n+1} = \mathbf{U}_i^n - \frac{\Delta t}{|\tau_i|} \sum_{j=1}^{3} \int_{\partial \tau_{i,j}} \mathbf{F}_j^*(\mathbf{U}_{\text{in}}^{n+1/2}, \mathbf{U}_{\text{out}}^{n+1/2}) \cdot \mathbf{n}_j ds + \Delta t \mathbf{S}_{b,i}^{n+1/2}, \tag{2.9}$$

where the numerical flux vector $\mathbf{F}^*(\mathbf{U}_{\text{in}}^{n+1/2}, \mathbf{U}_{\text{out}}^{n+1/2}) \cdot \mathbf{n}$ is calculated based on an approximate Riemann solver at each quadrature point on the cell boundary. The HLL approximate Riemann solver [22] is used in our implementation due to its simplicity and stable performance on wet/dry interface. $\nabla \mathbf{U}^{n+1/2}$ is taken as $\nabla \mathbf{U}^n$ instead of the reconstructed slope of $\mathbf{U}^{n+1/2}$, which gives much better numerical results [5] and saves the computational cost of an extra reconstruction.

The time step length Δt is determined by the CFL condition as

$$\Delta t = \text{CFL} \cdot \min_i \frac{\Delta x_i}{\sqrt{gh_i} + \sqrt{u_i^2 + v_i^2}}, \tag{2.10}$$

where Δx_i is the size of τ_i, usually computed as the minimum barycenter-to-barycenter distance between τ_i and its neighbor cells. In our simulations, the CFL number is always set as $\sqrt{2}/2$.

2.2. Linear reconstruction

In each time step, the cell mean value $\mathbf{U}_i^n$ is updated as $\mathbf{U}_i^{n+1}$ by (2.8) and (2.9). The slope of $\mathbf{U}_i^{n+1}$ is obtained by a piecewise linear reconstruction to achieve a 2nd order accuracy. Particularly, we use the Surface Gradient Method (SGM) [23] which suggests the reconstruction variables as $\eta = h + z$, hu and hv. With this method, one can preserve
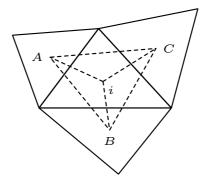
Figure 1: The ENO-type reconstruction on a patch of cells.

the lake at rest naturally for the case of continuous riverbed [23]. In our implementation, we use a simple ENO-type reconstruction method similar to [24] to suppress the numerical oscillations near steep gradients or discontinuities. Precisely, for a function $\phi = \eta$, hu or hv, with its cell mean value ϕ_i on τ_i given, the gradients of ϕ for the three triangles $\triangle AiB$, $\triangle BiC$ and $\triangle CiA$ are referred to as $(\nabla\phi)_{AiB}$, $(\nabla\phi)_{BiC}$ and $(\nabla\phi)_{CiA}$ (see Fig. 1), from which we choose the one with the minimal l^2 norm

$$\nabla\phi_i = \arg\min_{\nabla\phi}\Big\{\|\nabla\phi\|_{l^2}, \ \nabla\phi \in \big\{(\nabla\phi)_{AiB}, (\nabla\phi)_{BiC}, (\nabla\phi)_{CiA}\big\}\Big\}. \qquad (2.11)$$

Following the idea of minmod slope limiter, we set $\nabla\phi_i = 0$ when $\phi_i \geq \max\{\phi_A, \phi_B, \phi_C\}$ or $\phi_i \leq \min\{\phi_A, \phi_B, \phi_C\}$. In addition, the *physical criteria* should be satisfied in the process of reconstructing η, namely that the water depth $h = \eta - z$ must be non-negative at each quadrature points, otherwise $\nabla\eta_i$ is set to be zero.

Remark 2.1. After the piecewise linear reconstruction above, some of the cells is turned into the so-called partially wetted cells, saying the cells with water submerging at least one vertex but not all. For the partially wetted cells, the gradients of variables need to be fixed. For these cells, the general numerical techniques applied to wet cells are unable to produce qualitatively correct solutions, generating spurious velocities and often violating mass conservation [17]. We enforce zero gradients of both surface elevation and riverbed in partially wetted cells following [4, 16], which is the simplest method automatically capturing the wet/dry interface and preserving the still water state.

2.3. Hydro-static reconstruction

For the case of discontinuous riverbed, the hydro-static reconstruction method plus an additional correction of the source term [9] is adopted to preserve positivity of water depth and the lake at rest.

Along an edge of the cell τ_i, denote h_L, $u_{n,L}$, $q_{n,L}$, z_L and h_R, $u_{n,R}$, $q_{n,R}$, z_R as the left and right water depths, normal velocities, normal momentums and riverbed elevations in τ_i and its neighbour cell, respectively. The modified conservative variables are given below

for the numerical flux calculation

$$
\begin{cases}
z^* = \max(z_L, z_R), \\
h_L^* = \max(0, \eta_L - z^*), \quad h_R^* = \max(0, \eta_R - z^*), \\
\eta_L^* = h_L^* + z^*, \quad\quad\quad\; \eta_R^* = h_R^* + z^*, \\
q_L^* = u_L h_L^*, \quad\quad\quad\quad\; q_R^* = u_R h_R^*.
\end{cases}
\tag{2.12}
$$

Then the HLL numerical flux on this edge is modified to balance riverbed slope source term for the purpose of preserving the lake at rest,

$$
\mathbf{F}^* \cdot \mathbf{n} = \mathbf{F}_{\mathrm{HLL}} \cdot \mathbf{n} - \mathbf{SF}(\mathbf{U}_L^*) + \mathbf{SF}(\mathbf{U}_L),
\tag{2.13}
$$

with the static flux

$$
\mathbf{SF}(\mathbf{U}) = (0, gh^2 n_x/2, gh^2 n_y/2)^T,
$$

and the unit outward normal $\mathbf{n} = (n_x, n_y)^T$.

2.4. Boundary condition

We follow [6,25] to propose the boundary conditions. The characteristics theory tells us that the Riemann invariant $R^+ = u - 2\sqrt{gh}$ of the 1D SWEs is conserved along the right characteristics $dx/dt = u + \sqrt{gh}$, thus the open boundary condition for 2D SWEs is implemented based on Riemann invariants along the normal direction. In the following, we use subscripts n and τ to denote normal and tangential component, B and I to denote the values exterior and interior to the domain boundary. Let the Fround number to be $Fr = \sqrt{u^2 + v^2}/\sqrt{gh}$, the boundary condition we used is as

1. $Fr < 1$ (subcritical flow)

   The R^+ condition is given as

   $$
   u_{n,B} - 2\sqrt{gh_B} = u_{n,I} - 2\sqrt{gh_I}.
   \tag{2.14}
   $$

   Then we have

   $$
   u_{n,B} = u_{n,I} - 2\sqrt{g}(\sqrt{h_I} - \sqrt{h_B}), \quad h_B \text{ is prescribed;}
   \tag{2.15}
   $$

   or

   $$
   h_B = \left\{ \sqrt{h_I} - \frac{1}{2\sqrt{g}}(u_{n,I} - u_{n,B}) \right\}^2, \quad u_{n,B} \text{ is prescribed.}
   \tag{2.16}
   $$

   If the normal momentum $(hu)_{n,B}$ is prescribed, the substitution of $u_{n,B} = (hu)_{n,B}/h_B$ into Eq. (2.14) gives a nonlinear equation for h_B, which can be solved by an iterative method such as the Newton method.

2. $Fr > 1$ (supercritical flow)

   For inflow, the variables $h_B, u_{n,B}$ and $u_{\tau,B}$ are prescribed, and for outflow,

   $$
   h_B = h_I, \quad u_{n,B} = u_{n,I}, \quad u_{\tau,B} = u_{\tau,I}.
   \tag{2.17}
   $$

Another two types of boundary condition are applied at wall boundary, including the free slip boundary condition

$$h_B = h_I, \quad u_{n,B} = 0, \quad u_{\tau,B} = u_{\tau,I}, \tag{2.18}$$

and the reflective boundary condition

$$h_B = h_I, \quad u_{n,B} = -u_{n,I}, \quad u_{\tau,B} = u_{\tau,I}. \tag{2.19}$$

3. Friction source term of manning form

We discuss the stiffness of the friction source term of the Manning form in Subsection 3.1, then propose an direct integration method for the split equation (2.4b) in Subsection 3.2.

3.1. Stiffness of friction source term

The system (2.4b) for the friction source term of Manning form in component-wise formation is as

$$\begin{cases} \dfrac{\partial h}{\partial t} = 0, \\[2mm] \dfrac{\partial u}{\partial t} = -gn^2 h^{-4/3} u \sqrt{u^2 + v^2}, \\[2mm] \dfrac{\partial v}{\partial t} = -gn^2 h^{-4/3} v \sqrt{u^2 + v^2}. \end{cases} \tag{3.1}$$

Notice that h is invariant, we define $C(h) = gn^2 h^{-4/3}$ as a positive constant, then

$$\begin{cases} \dfrac{\partial u}{\partial t} = -C(h) u \sqrt{u^2 + v^2}, & \text{(3.2a)} \\[2mm] \dfrac{\partial v}{\partial t} = -C(h) v \sqrt{u^2 + v^2}. & \text{(3.2b)} \end{cases}$$

Let $\mathbf{q} = (u, v)^T$, $q_r = \sqrt{u^2 + v^2}$ and $\mathbf{\Phi}(u, v) = q_r \mathbf{q}$, then the Jacobian matrix $\mathbf{M} = \dfrac{\partial \mathbf{\Phi}}{\partial \mathbf{q}}$ has two eigenvalues q_r and $2q_r$.

The explicit, implicit or semi-implicit Euler scheme ($\beta = 0$, $\beta = 1$, $0 < \beta < 1$ respectively) applied to (3.2) is as

$$\mathbf{q}^{n+1} = \mathbf{q}^n - C(h)\Delta t \{(1-\beta)\mathbf{\Phi}^n + \beta \mathbf{\Phi}^{n+1}\}, \quad 0 \le \beta \le 1, \tag{3.3}$$

where $\mathbf{\Phi}^{n+1}$ is approximated by

$$\mathbf{\Phi}^{n+1} \approx \mathbf{\Phi}^n + \left(\frac{\partial \mathbf{\Phi}}{\partial \mathbf{q}}\right)^n (\mathbf{q}^{n+1} - \mathbf{q}^n) = q_r^n \mathbf{q}^n + \mathbf{M}^n (\mathbf{q}^{n+1} - \mathbf{q}^n),$$

which yields

$$\mathbf{q}^{n+1} = (\mathbf{I} + C(h)\Delta t \beta \mathbf{M}^n)^{-1} \{(1 - C(h)\Delta t q_r^n)\mathbf{I} + C(h)\Delta t \beta \mathbf{M}^n\} \cdot \mathbf{q}^n.$$

As the eigenvalues of $\mathbf{M}^n$ are q_r^n and $2q_r^n$, the classical stability condition of Euler schemes requires that

$$\begin{cases} |(1 + C(h)\Delta t \beta q_r^n)^{-1}\{1 - C(h)\Delta t q_r^n + C(h)\Delta t \beta q_r^n\}| < 1, & \text{(3.4a)} \\ |(1 + C(h)\Delta t \beta 2q_r^n)^{-1}\{1 - C(h)\Delta t q_r^n + C(h)\Delta t \beta 2q_r^n\}| < 1, & \text{(3.4b)} \end{cases}$$

which leads to

$$\begin{cases} C(h)\Delta t q_r^n(1 - 2\beta) < 2, & \text{(3.5a)} \\ C(h)\Delta t q_r^n(1 - 4\beta) < 2. & \text{(3.5b)} \end{cases}$$

Thus the necessary and sufficient conditions for the stability of scheme (3.3) are as

$$\begin{cases} \text{when } 0 \le \beta < \dfrac{1}{2}, \quad \text{stable} \iff \Delta t < \dfrac{2}{C(h)(1 - 2\beta)q_r^n}, \\ \text{when } \dfrac{1}{2} \le \beta \le 1, \quad \text{stable for all } \Delta t. \end{cases} \qquad \text{(3.6)}$$

In the case of $0 \le \beta < 1/2$, note that $C(h) \to +\infty$ as $h \to 0$. Thus we have $\Delta t \to 0$, provided that q_r^n has a positive lower bound. Therefore, if the explicit Euler scheme or the semi-implicit Euler scheme with $0 \le \beta < 1/2$ is applied, the time step Δt has to be much less than that given by the CFL condition (2.10) in the cell where the water depth h is very small, based on the requirement for numerical stability.

At the same time, the truncation error of the scheme (3.3) is

$$\mathcal{O}\big((-C(h)\Delta t)^{m+1}\big) = \mathcal{O}\big((h^{-4/3}\Delta t)^{m+1}\big), \qquad \text{(3.7)}$$

where m is accuracy order with $m = 2$ for $\beta = 1/2$ and $m = 1$ for other case. Therefore, the local truncation error of the Euler schemes is quite large in the vicinity of wet/dry interface where $h \to 0$, whatever the β takes.

3.2. Direct integration for friction source

To remove the stiffness and reduce the numerical error, we propose an analytical integration method below. The expression of analytical solution for Eq. (2.4b) is given below with initial values $\mathbf{U}_*^n = (h_*^n, (hu)_*^n, (hv)_*^n)$.

It is sufficient to solve Eq. (3.2). Taking $(3.2a) \times u + (3.2b) \times v$, we have

$$\frac{1}{2}\frac{\partial(u^2 + v^2)}{\partial t} = -C(h)(u^2 + v^2)^{3/2}. \qquad \text{(3.8)}$$

Let $q_r = \sqrt{u^2 + v^2}$. We have

$$\frac{\partial q_r}{\partial t} = -C(h)q_r^2. \qquad \text{(3.9)}$$

For initial value $\mathbf{U}_*^n = (h_*^n, (hu)_*^n, (hv)_*^n)$, the solution of (3.9) is as

$$\frac{q_r}{q_{r*}} = \frac{1}{1 + C(h_*^n)q_{r*}(t - t_*)}, \tag{3.10}$$

where $t - t_* = \Delta t$, $q_{r*} = \sqrt{(u_*^n)^2 + (v_*^n)^2}$. At the same time, the direction of velocity vector is preserved as $\frac{\partial(u/v)}{\partial t} = 0$, so we have $(u, v) = (u_*, v_*) \cdot \frac{q_r}{q_{r*}}$ and

$$\begin{cases} u^{n+1} = u_*^n / (1 + gn^2(h_*^n)^{-4/3}\sqrt{(u_*^n)^2 + (v_*^n)^2}\Delta t), \\ v^{n+1} = v_*^n / (1 + gn^2(h_*^n)^{-4/3}\sqrt{(u_*^n)^2 + (v_*^n)^2}\Delta t). \end{cases} \tag{3.11}$$

Therefore, we have the analytical solution for Eq. (2.4b) in the form of conservative variables as

$$\begin{cases} h^{n+1} = h_*^n, \\ (hu)^{n+1} = (hu)_*^n / (1 + gn^2(h_*^n)^{-7/3}\sqrt{((hu)_*^n)^2 + ((hv)_*^n)^2}\Delta t), \\ (hv)^{n+1} = (hv)_*^n / (1 + gn^2(h_*^n)^{-7/3}\sqrt{((hu)_*^n)^2 + ((hv)_*^n)^2}\Delta t). \end{cases} \tag{3.12}$$

This direct integration does not impose any constrain on the time step Δt, thus we completely remove the stiffness and get an absolutely stable method for the friction source term.

Remark 3.1. The friction source term involved in test case 5.1 has a simpler form with $C_D = \tau h / \sqrt{u^2 + v^2}$, thus

$$\mathbf{S}_f = \begin{pmatrix} 0 \\ -\tau hu \\ -\tau hv \end{pmatrix}, \tag{3.13}$$

where τ is the bed friction parameter. Similarly, we have the analytical solution for Eq. (2.4b) as

$$\begin{cases} h^{n+1} = h_*^n, \\ (hu)^{n+1} = e^{-\tau\Delta t}(hu)_*^n, \\ (hv)^{n+1} = e^{-\tau\Delta t}(hv)_*^n. \end{cases} \tag{3.14}$$

4. Overall truncation error

The overall truncation error of our method is coming from several folds. The first one is the spatial and temporal discretisation of the SWEs in Section 2. The second one is due to the time splitting and the last one is due to the treatment on the wet/dry boundary.

4.1. Time-splitting

We consider the Strang splitting (2.6) following [26]

$$\mathbf{U}(\mathbf{x}, t+\Delta t) \approx \exp\left(\frac{1}{2}\Delta t \mathscr{L}^F\right)\exp\left(\Delta t \mathscr{L}^I\right)\exp\left(\frac{1}{2}\Delta t \mathscr{L}^F\right)\mathbf{U}(\mathbf{x}, t), \qquad (4.1)$$

for the solution of $\frac{\partial \mathbf{U}}{\partial t} = (\mathscr{L}^I + \mathscr{L}^F)\mathbf{U}$, with $\mathscr{L}^I$ and $\mathscr{L}^F$ referring to (2.5a) and (2.5b).

If $\mathscr{L}^I$ and $\mathscr{L}^F$ are commutative, the splitting (4.1) is exact. Otherwise the splitting error operator is defined as

$$\begin{aligned}
E_{split}(\Delta t) &= \exp\left(\frac{1}{2}\Delta t \mathscr{L}^F\right)\exp\left(\Delta t \mathscr{L}^I\right)\exp\left(\frac{1}{2}\Delta t \mathscr{L}^F\right) - \exp\left(\Delta t(\mathscr{L}^I + \mathscr{L}^F)\right) \\
&= -\frac{1}{6}\Delta t^3\left(\frac{1}{4}(\mathscr{L}^F)^2\mathscr{L}^I - \frac{1}{2}\mathscr{L}^F\mathscr{L}^I\mathscr{L}^F + \frac{1}{4}\mathscr{L}^I(\mathscr{L}^F)^2 - \frac{1}{2}(\mathscr{L}^I)^2\mathscr{L}^F\right. \\
&\qquad \left. + \mathscr{L}^I\mathscr{L}^F\mathscr{L}^I - \frac{1}{2}\mathscr{L}^F(\mathscr{L}^I)^2\right) + \mathscr{O}(\Delta t^4).
\end{aligned} \qquad (4.2)$$

The truncation error operator for the Strang time-split method is (see [26] for details)

$$E^{Strang}(\Delta t) = E_{split}(\Delta t) + E_I(\Delta t) + 2E_F(\Delta t/2) + \mathscr{O}(\Delta t^4), \qquad (4.3)$$

where E_I and E_F are local truncation error operators for approximation solution operators of split equations (2.4a) and (2.4b), respectively.

In this work, we take advantage of the MUSCL-Hancock finite volume method to solve Eq. (2.4a), which is a 2nd-order upwind scheme of Godunov type, thus the truncation error $E_I(\Delta t) = \mathscr{O}(\Delta t^3)$. On the other hand, we solve Eq. (2.4b) by the analytical integration method, thus $E_F(\Delta t) = 0$. To examine the overall truncation error $E^{Strang}(\Delta t)$, the term remains to be checked is the norm of $\mathscr{L}^F$ as an operator on L^1 functions. Actually, we have

$$\begin{aligned}
\|\mathscr{L}^F\mathbf{U}\|_{L^1} &= \|C_D(0, u, v)^T\sqrt{u^2 + v^2}\|_{L^1} \\
&= \int_{\Omega, h>0} C_D(|u| + |v|)\sqrt{u^2 + v^2}dx \\
&\leq C\int_{\Omega, h>0} h^{-1/3}dx,
\end{aligned}$$

where u, v is assumed to be bound. Let us assume that there exists a constant $M > 0$ such that

$$\int_{\Omega, h>0} h^{-1/3}dx < M. \qquad (4.4)$$

Thus the total truncation L^1 error is $\mathscr{O}(\Delta t^3)$

$$\|E^{Strang}(\Delta t)\mathbf{U}\|_{L^1} < C\Delta t^3, \quad \text{if } \mathbf{U} \in L^1(\Omega). \qquad (4.5)$$

Remark 4.1. For the splitting error operator (4.2), a first glance gives $E_{split} = C_D^2 \mathcal{O}(\Delta t^3) = h^{-2/3}\mathcal{O}(\Delta t^3)$ with the assumption of boundness of velocities u and v, where the appearance of C_D is due to $\mathscr{L}^F$. As a result, we have

$$E^{Strang}(\Delta t) = h^{-2/3}\mathcal{O}(\Delta t^3), \tag{4.6}$$

which is clearly an improvement comparing to other numerical methods for the friction source term while $h \to 0$, such as the Euler scheme with truncation error $h^{-4}\mathcal{O}(\Delta t^3)$ for $\beta = 1/2$ in Eq. (3.7).

Remark 4.2. It is clear that the assumption (4.4) is invalid if there is a wet part with very thin layer of water. Here we put a few words on how severe a constraint the assumption (4.4) exerts on the solution. For 1D case, considering the case that the wet/dry interface locates at $x = 0$ and $h = x^\alpha$, we then have

$$\int_0^1 h^{-1/3}dx = \int_0^1 x^{-\alpha/3}dx < \infty$$

requires that $\alpha < 3$.

4.2. Wet/dry tracking

The cells with water depth $h < h_{tol}$ are taken as dry cells, where the cell mean momentums are cleared to be zero. There are no numerical fluxes between dry cells. Namely, we modify numerical solution $\mathbf{U}^n = (h^n, (hu)^n, (hv)^n)$ at the n-th time step to

$$\hat{\mathbf{U}}^n = \begin{cases} (h^n, 0, 0), & \text{if } h^n < h_{tol}, & \text{(4.7a)} \\ \mathbf{U}^n, & \text{otherwise.} & \text{(4.7b)} \end{cases}$$

We assume that the velocities u, v is uniformly bounded following the physical common sense, which leads to

$$\hat{\mathbf{U}}^n - \mathbf{U}^n < Ch_{tol}. \tag{4.8}$$

It is clear we have the following:

Proposition 4.1. If h_{tol} is taken as

$$h_{tol} = \mathcal{O}(\Delta x^2), \tag{4.9}$$

and the area of the domain where $0 < h < h_{tol}$ is assumed to be $\mathcal{O}(\Delta x)$, then the truncation L^1 error is of $\mathcal{O}(\Delta x^3)$.

The domain where $0 < h < h_{tol}$ is assumed to be the narrow band in the vicinity of wet/dry boundary with length $\mathcal{O}(1)$ and band width $\mathcal{O}(\Delta x)$, thus its area is of order $\mathcal{O}(\Delta x)$. Then the L^1 truncation error due to modification Eq. (4.7) is obviously $\mathcal{O}(\Delta x^3)$.

Remark 4.3. If the system is solved on an h-type adaptive mesh, the dependence of h_{tol} on Δx can be local since Δx is not a constant over the computational domain. Based on our experience, we take h_{tol} in a cell as the following empirical form

$$h_{tol} = \epsilon h_c \min\left(\frac{\Delta x}{\Delta x_{ref}}, 1\right)^2, \tag{4.10}$$

where ϵ is a small number (we set it to be around 10^{-3} in the implementation), h_c is the typical water depth, which is usually taken as the maximum water depth in initial conditions and boundary conditions, Δx is the size of the cell, and Δx_{ref} is the reference cell scale which can be set to be the minimum mesh scale $\Delta x_{\min}$ of the initial mesh for example.

5. Numerical tests

In this section, we present several numerical tests to validate the 2nd-order convergence of our scheme, the effectiveness of our choice of h_{tol} and the analytical integration method for the friction terms, then we simulate the river flow on a complex rough topography. The numerical scheme is implemented using C++ programming language based on the adaptive finite element package AFEPack [27]. The h-type adaptive mesh technique and parallelization on distributed memory architecture are used.

In our simulation, the order of convergence α is defined by

$$E \approx N^{-\frac{\alpha}{D}},$$

where the error E is computed in L^1 norm, N is the number of cells and $D = 2$ is the dimension of domain. Thus

$$\alpha = -D \times s, \tag{5.1}$$

where s is the asymptotic slope in the log-log map of E versus N, which is expected to be -1.

For test Cases 5.2 and 5.4, the technique of mesh adaptation is introduced to tackle the issue that a loss of convergence order generally occurs on uniformly refined meshes due to the presence of steep gradients or genuine discontinuities. The h-adaptive methods on unstructured mesh are based on information retrieved from *a posteriori* error estimators which are derived from local error analysis. The heuristic local error indicator adopted in our computation is given as

$$\mathscr{E}_\tau = \mathscr{E}_\tau(\eta) + \mathscr{E}_\tau(hu) + \mathscr{E}_\tau(hv) + \mathscr{E}_\tau(z), \tag{5.2}$$

where

$$\mathscr{E}_\tau(\phi) = |\tau| \int_{\partial\tau} \frac{1}{\sqrt{|\tau|}} |[\![I_h\phi]\!]| + |[\![\nabla I_h\phi]\!]| \, \mathrm{d}\mathbf{l}, \tag{5.3}$$

where τ is a cell in the mesh and $|\tau|$ is its area, $[\![\cdot]\!]$ denotes the jump of a variable across $\partial\tau$, and $I_h\phi$ is the piecewise linear numerical solution for ϕ, with $\phi = \eta, hu, hv, z$. We refer to [28] and [29] for details of h-adaptive method and Eq. (5.3), respectively.

5.1. Test case 1: oscillatory flow above parabolic bottom topography

This classic test of oscillatory flow above parabolic bottom topography with analytical solution was first proposed by Thacker [30] including Coriolis force terms, then extended by Sampson et al. [31] including friction terms instead, and recently extended to 2D case by Wang et al. [32].

The 2D parabolic bed topography is

$$z_b(x, y) = h_0(x^2 + y^2)/a^2,$$

where h_0 and a are both constants. The friction terms take the following simpler expression (3.13) instead of Manning form (2.3), see Remark 3.1. The analytical solution depends on the relationship between τ and a peak amplitude parameter

$$p = \sqrt{8gh_0/a^2}.$$

Here we only consider the case of $\tau < p$ and the exact solution is

$$\eta(x, y, t) = h_0 - \frac{1}{2g}B^2 e^{-\tau t} - \frac{1}{g}Be^{-\tau t/2}\left(\frac{\tau}{2}\sin(st) + s\cos(st)\right)x$$
$$+ \frac{1}{g}Be^{-\tau t/2}\left(\frac{\tau}{2}\cos(st) - s\sin(st)\right)y, \tag{5.4}$$

and

$$u(t) = Be^{-\tau t/2}\sin(st), \qquad v(t) = -Be^{-\tau t/2}\cos(st), \tag{5.5}$$

where B is a constant and $s = \sqrt{p^2 - \tau^2}/2.$[†]

The computational domain is $[-5000m, 5000m] \times [-5000m, 5000m]$, and discretized into 28672 uniform cells with minimum mesh scale $36.25m$. The constants are set as $h_0 = 10m, a = 3000m, B = 5m/s$. For a non-frictional flow, $\tau = 0$, and the flow is expected to indefinitely oscillate inside the parabolic basin with a half-period of $T/2 = 672.8s$. For a frictional flow, it is assumed that $\tau = 0.002s^{-1}$. The simulation is carried out for four periods until $t = 4T = 5382.4s$ for both cases. The boundary conditions are transmissive which have no influence on the flow as it never reaches the boundary. We take $h_c = h_0$ and $\Delta x_{ref} = 36.25$ in the Eq. (4.10) to give h_{tol}. The CFL number is set as $\sqrt{2}/4$ for this test case.

Figs. 2 and 3 show the numerical results in terms of velocity time histories at a point $(1000, 0)$ and a water surface profile along line $y = 0$ at $t = T/2$ and $4T$. The numerical results are in perfect agreement with the exact solution and the moving wet-dry fronts are well resolved.

[†]We have found that actually the results in Wang et al. [32] are incorrect as the error of two components of the velocity are not on the same level. It looks that the problem is due to a typo in the analytical expression of the solution, i.e., the sign of the last term of Eq. (5.4) is incorrectly negative in [32].
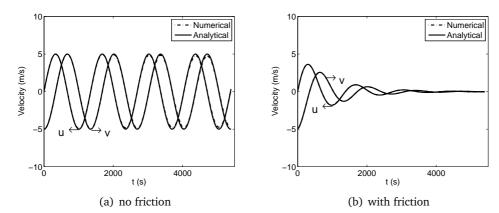
(a) no friction   (b) with friction

Figure 2: Test case 5.1, velocity time histories at the point $(1000, 0)$.

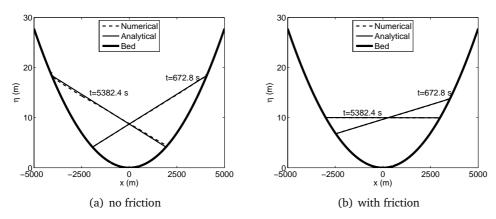(a) no friction   (b) with friction

Figure 3: Test case 5.1, the water level profile along line $y = 0$ at $t = T/2$ and $4T$.

5.2. Test case 2: dam-break wave propagating over three humps with friction

This case of dam-break water waves over the dry riverbed with three humps was first studied by Kawahara and Umetsu [33] and reconsidered by other authors (e.g., [4, 34]), in order to verify the capacity of the numerical method in predicting flow over uneven topography with wetting and drying. The computational domain is $[0m, 75m] \times [0m, 30m]$, with the bed topography defined by

$$z(x, y) = \max \left\{ 0, \ 1 - \frac{1}{8} \sqrt{(x - 30)^2 + (y - 6)^2}, \ 1 - \frac{1}{8} \sqrt{(x - 30)^2 + (y - 24)^2}, \right.$$
$$\left. 3 - \frac{3}{10} \sqrt{(x - 47.5)^2 + (y - 15)^2} \right\}.$$

The Manning coefficient n is 0.018. In the formula (4.10) for h_{tol}, we take $h_c = 2$ and $\Delta x_{ref} = 1.065$ as the minimum mesh scale of the initial mesh of 557 cells. The slip boundary conditions are applied at all the boundaries.

(a) $t = 3s$ (b) $t = 6s$

(c) $t = 12s$ (d) $t = 30s$

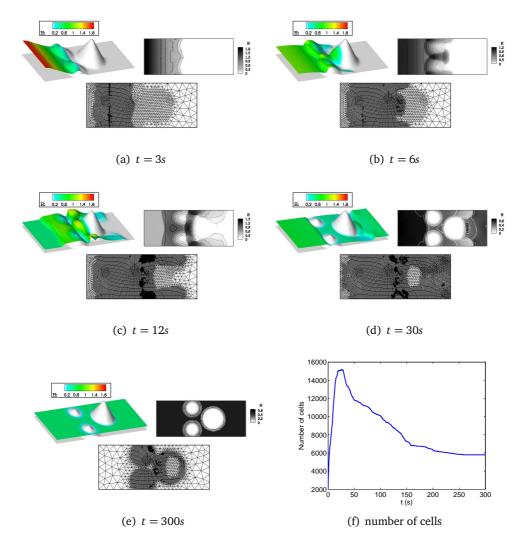(e) $t = 300s$ (f) number of cells

Figure 4: Test case 5.2: water surface elevation, water depth contour and adaptive meshes at different times and time histories of the total number of cells.

Initially, the dam is situated at $x = 16\ m$ containing still water with surface elevation $\eta = 1.875\ m$, then it collapses at $t = 0s$. Fig. 4 shows the propagation of the flood at several moments, where the 3D visualisations of water surface elevation, plan views of water depth contour and adaptive meshes are represented. The numerical results are obtained with the initial adaptive mesh with 2191 cells and the initial adaptive tolerance as 0.05. At $t = 3s$, the flow has reached the tops of two small hills and begins to rise over them. At $t = 6s$, the small hills are totally submerged and the flow front reaches more than halfway up the large hill. Then at $t = 12s$, it fails to reach the top, passes through two sides of the large hill to the back. After complicated wave-wave, wave-wall, wave-topography interactions and the dissipated effect of friction force, the flow finally reaches a steady state
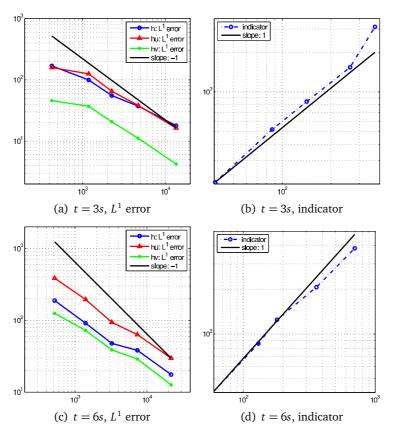
(a) $t = 3s$, L^1 error   (b) $t = 3s$, indicator

(c) $t = 6s$, L^1 error   (d) $t = 6s$, indicator

Figure 5: Test case 5.2: the log-log map of the L^1 error of h, hu, hv on adaptively refined meshes against the number of cells and the log-log map of the indicator against the L^1 error at $t = 3s$ and $6s$.

with still water at $t = 300s$. The numerical model simulates well the complicated process of wetting and drying. The time evolution of the number of cells in the adaptive meshes is shown in Fig. 4(f).

The numerical solutions are also computed on a series of adaptive meshes, with the adaptive tolerance decreasing from an initial value of 5 to $5/2^8$. The reference solution is computed on a uniform mesh with $223,232$ cells. The convergence results are shown in Fig. 5. It reveals that our numerical scheme achieves almost optimal 2nd-order accuracy at both $t = 3s$ and $6s$. The indicator is proportional to the L^1 error both at $t = 3s$ and $6s$.

5.3. Test case 3: Malpasset dam-break

In 1959, the Malpasset dam broke on the Reyan River valley in the southern France, which was a rare example of total and instantaneous collapse of an arch dam, and was responsible for more than 400 injuries. After the disastrous event, laboratory studies were carried out by Electricité de France (EDF) to measure the arrival time and maximum water level at several gauge points (for the coordinates of these points we refer to Hervouet [35]).
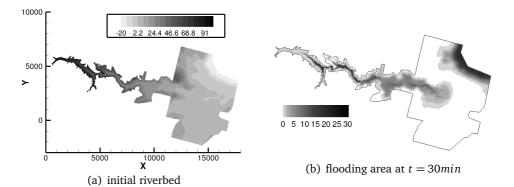
(a) initial riverbed

(b) flooding area at $t = 30min$

Figure 6: Test case 5.3, initial riverbed and flooding area at $t = 30min$.
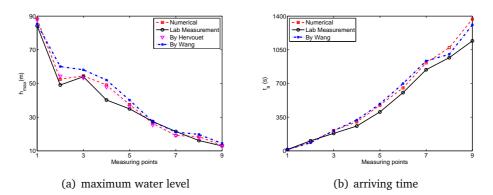

(a) maximum water level

(b) arriving time

Figure 7: Test case 5.3: comparison of numerical results with those given by Hervouet [35] and Wang et al. [32] and laboratory data at various measuring points.

Many authors (e.g., [7, 32, 35, 36]) have studied this case and we revisit it here to validate our model.

The simulation is performed on a non-uniform triangulated mesh with 26011 cells with the same mesh points as [35]. The dimensions are $17500m \times 9000m$ and the minimum mesh scale is $3.304m$, see Fig. 6. The dam is modelled by a straight line formed by points $D_1(4701.183m, 4143.407m)$ and $D_2(4655.553m, 4392.104m)$. Initially, it is assumed that the water level is $100m$ upstream and the floodplain downstream is dry. The manning coefficient is set to $n = 0.033s/m^{1/3}$ as [32]. The upstream boundary conditions are set to be $h, u, v = 0$, $z = 100$ and the other downstream boundaries are transmissive. For h_{tol}, it is taken that $h_c = 100$ and $\Delta x_{ref} = 3.3$ in the formula Eq. (4.10).

Fig. 6 shows the elevation of riverbed and the flooding extent at $t = 30$ min when the water has already inundated a wide area downstream. Fig. 7 gives the comparison of numerical results and experimental data obtained from the physical experiment in terms of arriving time and maximum water depth, at various gauge points downstream, resulting in satisfactory agreement. Our results fit quite well with the experimental data and the numerical results given by Hervouet [35] and Wang et al. [32].

5.4. Three Gorges dam-break simulation

As the last example, we simulate the inundation by the Three Gorges dam-break in the Yangtze River physical model, with the purpose of studying the robustness of our method when handling large scale problem with complex rough topography. The Three Gorges dam was built at Sandouping Town, Zigui County, 38 km upstream of Yichang City with area about 90 km^2 and population 1.6 million, see Fig. 8. The Three Gorges dam was built with the design elevation as 181 meters, the maximal water level as 175 meters, and the crest of inflow discharge to be $m_{max} = 7 \times 10^4 m^3/s$. It forms a reservoir of $3.93 \times 10^{10} m^3$.

Figure 8: The location of the Three Gorges dam and Yichang City in Google Map.

The computational domain is taken to be a part of Yangtze River basin containing the Three Gorges dam. The initial state is shown in Fig. 9(a), where the water is at rest with surface elevation $175m$ upstream of the dam and the floodplain downstream is dry. The inflow velocity is set as $v_0 = 3m/s$ and the inflow water surface elevation $\eta_0 = 223\ m$, so that the total inflow discharge is numerically integrated to be $7.0059 \times 10^4 m^3/s$ closely approaching the crest one m_{max}. The inflow and outflow boundaries lie on the up-left and down-right side of the computational domain, respectively. The reflective boundary conditions are simply taken at the outflow boundary and other lateral boundaries, where the cells are not much interested by the flow and therefore the related boundary conditions have little influence on the results. The Manning coefficient n is 0.018. In the formula (4.10) for h_{tol}, we take $h_c = 223$ as the inflow water surface elevation and $\Delta x_{ref} = 76.635$ as the mesh scale of an initial uniform mesh of 37704 cells.

The technique of mesh adaption is used to improve the computational efficiency, with

(a) initial state
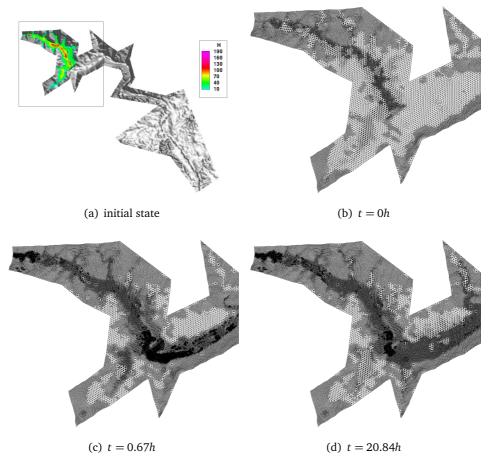
(b) $t = 0h$

(c) $t = 0.67h$

(d) $t = 20.84h$

Figure 9: The Three Gorges dam-break simulation: (a) is the computational domain and the initial state with color representing the value of water depth. (b), (c) and (d) are the adaptive mesh in the up-left domain at $t = 0$, 0.67, 20.84 hours.

adaptive tolerance 5×10^5, see Figs. 9(b)-9(d) for the adaptive meshes in the up-left part of the domain at different times.

At the beginning, the water cascades down due to the fall head of water surface on two sides of the dam, then rushes through the grand zigzag gorge between high mountains, passes through the first third of grand gorge at about $t = 0.67$ hours, the second third at about $t = 2.07$ hours, flowing backward to several tributaries along the gorge, and finally bursts out the exit of the gorge at $t = 5.27$ hours, see Figs. 10(b)-10(d). The flow velocity is turning slower, partially due to the fact that the topography elevation gets higher along the gorge, especially near the sharp bend at the second third of grand gorge. In our simulation, the water then pours into Yichang City 5.27 hours after the dam-break. Almost half the city is submerged by the flood at $t = 11.11$ hours, while all the city and villages nearby are overwhelmed at $t = 20.84$ hours, see Figs. 11 and 12.

(a) $t = 0h$ (b) $t = 0.67h$

(c) $t = 2.07h$ (d) $t = 5.27h$
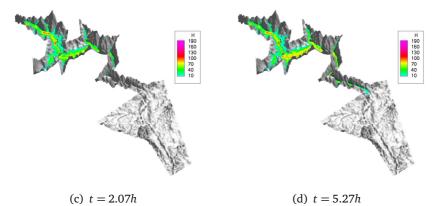
Figure 10: The Three Gorges dam-break simulation: the water depths at $t = 0$, 0.67, 2.07 and 5.27 hours.
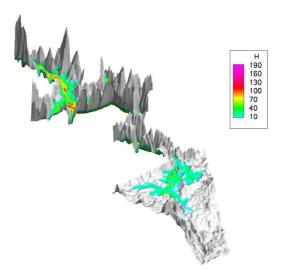

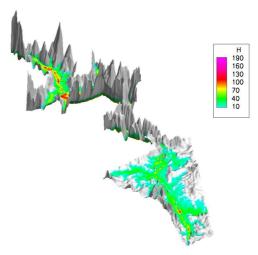Figure 11: The Three Gorges dam-break simulation: the water depths at 11.11 hours.

Figure 12: The Three Gorges dam-break simulation: the water depths at 20.84 hours.

6. Conclusions

We proposed a robust numerical scheme to solve the shallow water equations with friction source term on complex rough topography. We adopted a time splitting scheme to separate the friction source term and derived a direct integration formula to handle it that the stiffness due to the friction is elevated. With a moderate setup of the water depth tolerance, the overall truncation error of the scheme is of 2nd order accuracy. The water depth tolerance is essentially problem independent and a refined formula based on our experience of this parameter is helpful to improve the numerical performance. With the help of these two points, the behaviors of the numerical scheme is very robust, and the numerical instabilities as reported in the literatures are erased. The scheme is coupled with h-adaptive mesh technique to carry out numerical simulations on several different cases with satisfied accuracy and stability.

References

[1] T. MOLLS, G. ZHAO, AND F. MOLLS, *Friction slope in depth-averaged flow*, Journal of Hydraulic Engineering, 124(1) (1998), pp. 81–85.

[2] S. F. BRADFORD AND B. F. SANDERS, *Finite-volume model for shallow-water flooding of arbitrary topography*, Journal of Hydraulic Engineering, 128(3) (2002), pp. 289–298.

[3] A. Valiani and L. Begnudelli, *Divergence form for bed slope source term in shallow water equations*, Journal of Hydraulic Engineering, 132(7) (2006), pp. 652–665.

[4] Q. Liang and A. G. L. Borthwick, *Adaptive quadtree simulation of shallow flows with wet-dry fronts over complex topography*, Computers and Fluids, 38(2) (2009), pp. 221–234.

[5] K. Hu, C. G. Mingham, and D. M. Causon, *Numerical simulation of wave overtopping of coastal structures using the non-linear shallow water equations*, Coastal Engineering, 41(4) (2000), pp. 433–465.

[6] T. H. Yoon and S. K. Kang, *Finite volume model for two-dimensional shallow water flows on unstructured grids*, Journal of Hydraulic Engineering, 130(7) (2004), pp. 678–688.

[7] A. Valiani, V. Caleffi, and A. Zanni, *Case study: Malpasset dam-break simulation using a two-dimensional finite volume method*, Journal of Hydraulic Engineering, 128(5) (2002), pp. 460–472.

[8] K. Anastasiou and C. T. Chan, *Solution of the 2D shallow water equations using the finite volume method on unstructured triangular meshes*, International Journal for Numerical Methods in Fluids, 24(11) (1997), pp. 1225–1245.

[9] E. Audusse, F. Bouchut, M. O. Bristeau, R. Klein, and B. Perthame, *A fast and stable well-balanced scheme with hydrostatic reconstruction for shallow water flows*, SIAM Journal on Scientific Computing, 25(6) (2004), pp. 2050–2065.

[10] A. Kurganov and G. Petrova, *A second-order well-balanced positivity preserving central-upwind scheme for the Saint-Venant system*, Communications in Mathematical Sciences, 5(1) (2007), pp. 133–160.

[11] M. J. Castro, J. M. González-Vida, C. Parés, and N. Bellomo, *Numerical treatment of wet/dry fronts in shallow flows with a modified Roe scheme*, Mathematical Models and Methods in Applied Sciences, 16(6) (2006), pp. 897–932.

[12] M. Ricchiuto and A. Bollermann, *Stabilized residual distribution for shallow water simulations*, Journal of Computational Physics, 228(4) (2009), pp. 1071–1115.

[13] A. Bollermann, S. Noelle, and M. Lukáčová-Medvid'ová, *Finite volume evolution Galerkin methods for the shallow water equations with dry beds*, Communications in Computational Physics, 10(2) (2011), pp. 371–404.

[14] J. M. Gallardo, C. Parés, and M. Castro, *On a well-balanced high-order finite volume scheme for shallow water equations with topography and dry areas*, Journal of Computational Physics, 227(1) (2007), pp. 574–601.

[15] S. F. Bradford and N. D. Katopodes, *Hydrodynamics of turbid underflows. I: Formulation and numerical analysis*, Journal of Hydraulic Engineering, 125(10) (1999), pp. 1006–1015.

[16] P. Brufau and P. García-Navarro, *Unsteady free surface flow simulation over complex topography with a multidimensional upwind technique*, Journal of Computational Physics, 186(2) (2003), pp. 503–526.

[17] L. Begnudelli and B. F. Sanders, *Unstructured grid finite-volume algorithm for shallow-water flow and scalar transport with wetting and drying*, Journal of Hydraulic Engineering, 132(4) (2006), pp. 371–384.

[18] C. B. Vreugdenhil, Numerical Methods for Shallow-Water Flow, Springer, 1994.

[19] M. H. Tseng, *Improved treatment of source terms in TVD scheme for shallow water equations*, Advances in Water Resources, 27(6) (2004), pp. 617–629.

[20] G. Strang, *On the construction and comparison of difference schemes*, SIAM Journal on Numerical Analysis, 5(3) (1968), pp. 506–517.

[21] G. D. Van Albada, B. Van Leer, and Jr. W. W. Roberts, *A comparative study of computational methods in cosmic gas dynamics*, Astronomy and Astrophysics, 108 (1982), pp. 76–84.

[22] A. Harten, P. D. Lax, and B. Van Leer, *On upstream differencing and Godunov-type schemes for*

hyperbolic conservation laws, SIAM Review, (1983), pp. 35–61.

[23] J. G. Zhou, D. M. Causon, C. G. Mingham, and D. M. Ingram, *The surface gradient method for the treatment of source terms in the shallow-water equations*, Journal of Computational Physics, 168(1) (2001), pp. 1–25.

[24] R. Abgrall, *On essentially non-oscillatory schemes on unstructured meshes: analysis and implementation*, NASA Contractor Report 191415 (1992).

[25] P. A. Sleigh, P. H. Gaskell, M. Berzins, and N. G. Wright, *An unstructured finite-volume algorithm for predicting flow in rivers and estuaries*, Computers and Fluids, 27(4) (1998), pp. 479–508.

[26] R. J. LeVeque and J. Oliger, *Numerical methods based on additive splittings for hyperbolic partial differential equations*, Mathematics of Computation, 40(162) (1983), pp. 469–497.

[27] R. Li and W. B. Liu, http://dsec.pku.edu.cn/~rli/.

[28] R. Li, *On multi-mesh h-adaptive methods*, Journal of Scientific Computing, 24(3) (2005), pp. 321–341.

[29] R. Li, and S.-N. Wu, *H-adaptive mesh method with double tolerance adaptive strategy for hyperbolic conservation laws*, DOI: 10.1007/s10915-013-9692-1, 2013.

[30] W. C. Thacker, *Some exact solutions to the nonlinear shallow-water wave equations*, Journal of Fluid Mechanics, 107(1) (1981), pp. 499–508.

[31] J. Sampson, A. Easton, and M. Singh, *Moving boundary shallow water flow above parabolic bottom topography*, ANZIAM Journal, 47 (2006), pp. C373–C387.

[32] Y. Wang, Q. Liang, G. Kesserwani, and J. W. Hall, *A 2D shallow flow model for practical dam-break simulations*, Journal of Hydraulic Research, 49(3) (2011), pp. 307–316.

[33] M. Kawahara and T. Umetsu, *Finite element method for moving boundary problems in river flow*, International Journal for Numerical Methods in Fluids, 6(6) (1986), pp. 365–386.

[34] P. Brufau, M. E. Vázquez-Cendón, and P. García-Navarro, *A numerical model for the flooding and drying of irregular domains*, International Journal for Numerical Methods in Fluids, 39(3) (2002), pp. 247–275.

[35] J.M.Hervouet, Hydrodynamics of Free Surface Flows: Modelling with the Finite Element Method, John Wiley & Sons Inc, 2007.

[36] J. M. Hervouet and A. Petitjean, *Malpasset dam-break revisited with two-dimensional computations*, Journal of Hydraulic Research, 37(6) (1999), pp. 777–788.